1328

Chem. Eng. Technol. **2008**, *31*, No. 9, 1328–1335

Mei Liu[1]

Jinlong Zhang[1]

Yu Liu[1]

W. M. Lau[2]

Jun Yang[1]

[1] Department of Mechanical and Materials Engineering, University of Western Ontario, Canada.

[2] University of Western Ontario, Canada.

Research Article

Modeling of Flow Burst, Flow Timing in Lab-on-a-CD Systems and Its Application in Digital Chemical Analysis

A theoretical model is developed to predict the time-dependent behaviors of "flow burst" and centrifugal capillary flow in Lab-on-a-CD systems. Enabling the calculation of flow field, flow burst, and flow timing as a function of fluid properties and system specifications, the model is a useful design tool for understanding and controlling flow behaviors in Lab-on-a-CD devices. More importantly, the model shows great promise in the development of a new method for digital chemical analysis.

1 Introduction

Lab-on-a-chip or micro Total Analysis Systems (μTAS) has been leading a revolution in chemistry and biology for the past decade [1–4]. Control of microflows is the main issue in this field. Several methods of flow control have been developed in microfluidic systems, such as mechanical pumping, electrokinetic driving, capillary force directing, and thermal control. Lab-on-a-CD (Compact Disc) is another major form of Lab-on-a-chip technology. The most attractive advantage of this technique is its simple driving mechanism which reduces the need for an external pumping system. By spinning a CD, a centrifugal force is developed along the radial direction from the center of rotation to the edge of the CD. Thus the resulting body force, centrifugal force, is able to drive various liquids flowing in microchannel networks placed on the CD. Such Lab-on-a-CD platforms have achieved several microfluidic functions including capillary valving, centrifugal pumping, Coriolis force based switching, flow sequencing, and flow metering [5–13]. With this simple method of propulsion, Lab-on-a-CD could be easily adapted to numerous applications in the fields of chemistry, material science, and biotechnology [5–16].

Due to system rotation, centrifugal flows experience two-body forces: centrifugal force and Coriolis force. As shown in Fig. 1a), the centrifugal force, f_ω[1], is along the radial direction

and the Coriolis force, f_c, is perpendicular to the flow direction. Because of the existence of the two-body forces, centrifugal flows can become quite complex. Macroscale flows in rotating channels have been investigated experimentally by Benton and Boyer [17], and Ram [18], theoretically by Baura [19] and Benton [20], and numerically by Yang and Kim [21], and Lei and Hsu [22]. Lei and Hsu [22] defined two dimensionless numbers: the rotational Reynolds number, R_ω ($= \omega a^2/v$, where ω, a, and v are the angular velocity of rotation, the characteristic size of the channel and the kinematic viscosity of the fluid, respectively), and the reduced pressure gradient, G ($= G^* a^3/\rho v^2$, where G^* is the reduced pressure gradient and ρ is the
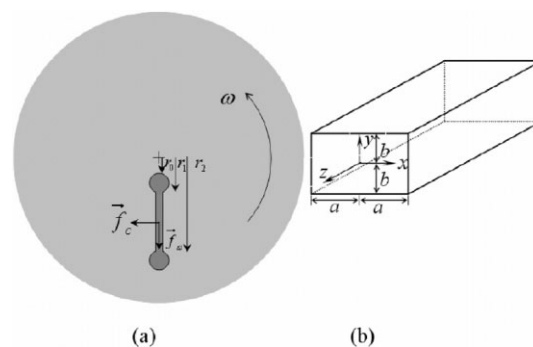

Figure 1. (a) An illustrative model for the forces acting on the liquid mass inside a microchannel on a CD spinning anti-clockwise with an angular velocity, ω. f_ω and f_c are the centrifugal force and Coriolis force densities, respectively. r_0, r_1, and r_2 are the distances of the inner reservoir, the entrance of the microchannel, and end of the microchannel to the center of rotation, respectively. (b) Geometric characteristics of the microchannel with the associated local Cartesian coordinate system, $z = 0$ is set at the entrance of the microchannel.

Correspondence: Assis. Prof. J. Yang (jyang@eng.uwo.ca), Department of Mechanical and Materials Engineering, University of Western Ontario, London, ON, N6A 5B9, Canada.

1) List of symbols at the end of the paper.

Chem. Eng. Technol. **2008**, *31*, No. 9, 1328–1335

Lab-on-a-CD systems   1329

fluid density). They suggested that the secondary flow is too weak to modify the primary flow along the axial direction of the channel when $R_\omega \leq 10$ and $R_\omega G \leq 100$, so that the axial velocity profile remains the standard parabolic profile of the Poiseuille flow and the secondary flow is negligible. Particularly for microchannel flows in Lab-on-a-CD systems, Madou et al. proved experimentally that the pressure gradient inside a CD-based microchannel flow is linear and the Hagen-Poiseuille equation is sufficient to estimate the flow rate [5]. Similar experiments have also been conducted by Duffy and coworkers [6] in their centrifugal microfluidic systems. They found that CD-based microchannel flows are indeed Hagen-Poiseuille flows for a wide range of attributes, including angular velocity from 400 to 1600 rpm, microchannel size from 20 to 500 µm, and viscosity from 1 to 10 times of the viscosity of water. In their experiments, the range of flow parameters covers most applications of microchannel flows in Lab-on-a-CD systems. Thus, in practice, CD-based microchannel flows are normally treated as Hagen-Poiseuille flows.

Reliable modeling tools of time-dependent centrifugal microflows are able to optimize design of Lab-on-a-CD devices in terms of flow volume control, flow timing, and flow sequencing. However, no comprehensive analysis on time-dependent centrifugal microflows has been conducted, particularly for the experimentally observed flow "burst" and capillary microflows. Here, a theoretical model is proposed to describe time-dependent centrifugal microflows in a straight rectangular microchannel. In the following sections, i) analytical solutions of continuous centrifugal microflows in a rectangular microchannel are obtained; ii) resulting pressure distribution inside the microchannel is determined; iii) a model is created to describe a centrifugal capillary microflow with a moving front in the microchannel, which is essential to understand time-dependent loading processes. In this model, a dynamic contact angle is taken into account. Based on the model, a novel concept of digital flow control in Lab-on-a-CD systems is proposed.

2 Theoretical Analyses

2.1 Time-Dependent Centrifugal Flow in a Rectangular Microchannel

A laminar, time-dependent, centrifugal flow in a straight rectangular microchannel is studied which connects two reservoirs on a spinning CD (Fig. 1a)). Two coordinate systems are used: one is the global polar coordinate system (Fig. 1a)); the other is the local Cartesian coordinate system (Fig. 1b)) where the z-axis is taken to coincide with the microchannel central axis, which is in the radial direction of the global polar coordinate system. The velocity component in the z direction, V_z, is considered here only since the secondary flow (V_x and V_y) is negligible. In addition, the Coriolis force along the z direction due to the secondary flow has a negligible effect on the main flow, V_z, as well. Due to flow continuity, V_z should be independent of z. Thus, in the local Cartesian coordinate system, the Navier-Stokes equation, the initial condition, and no-slip boundary conditions imposed on $V_z(x, y, t)$ are:

$$\frac{1}{v}\frac{\partial V_z(x,y,t)}{\partial t} = \frac{1}{\eta}\left(-\frac{dp}{dz} + f_\omega\right) + \frac{\partial^2 V_z(x,y,t)}{\partial x^2} + \frac{\partial^2 V_z(x,y,t)}{\partial y^2}$$

$$V_z(x,y,0) = 0,$$

$$V_z(\pm a, y, t) = 0, \quad V_z(x, \pm b, t) = 0$$

$$(1)$$

where η, ρ, $v\ (= \eta/\rho)$, $-dp/dz$, f_ω, a and b are the liquid viscosity, liquid density, liquid kinematic viscosity, pressure gradient along the microchannel, centrifugal force density, half of the width, and half of the height of the rectangular channel, respectively. Before the CD spins, there is no flow so that the initial velocity is zero.

At a constant angular velocity, the centrifugal force density, f_ω, depends on z only and can be expressed as:

$$f_\omega = r\omega^2 r = r\omega^2 (r_1 + z)$$

$$(2)$$

where ω and r are the angular velocity and the distance of a liquid element from the rotation center, respectively. Hence, the term $-dp/dz + f_\omega$ also depends on z only. By solving the Navier-Stokes equation in Eq. (1) using Green's functions [23, 24], the solution of velocity, V_z, can be obtained:

$$V_z(x,y,t) = \frac{16}{\pi^2\eta}\left(-\frac{dp}{dz} + f_\omega\right)$$

$$\sum_{m=1}^{\infty}\sum_{n=1}^{\infty}\frac{(-1)^{m+n}}{(2m-1)(2n-1)\lambda_{m,n}}\left[1 - e^{-\lambda_{m,n}vt}\right]\cos\frac{\beta_m x}{a}\cos\frac{\beta_n y}{b}$$

$$(3)$$

where $\lambda_{m,n} = \frac{\beta_m^2}{a^2} + \frac{\beta_n^2}{b^2}$, $\beta_m = \pi(m - \frac{1}{2})$ and $\beta_n = \pi(n - \frac{1}{2})$.

The flow rate is thus described by the following equation:

$$Q_t = \int_{-a}^{a}\int_{-b}^{b} V_z(x,y)dxdy = \frac{256ab}{\pi^4\eta}\left(-\frac{dp}{dz} + f_\omega\right)$$

$$\sum_{m=1}^{\infty}\sum_{n=1}^{\infty}\frac{1 - e^{-\lambda_{m,n}vt}}{(2m-1)^2(2n-1)^2\lambda_{m,n}}$$

$$(4)$$

Typically, the development of a centrifugal microflow to its steady state takes a short period of time, normally on the order of milliseconds. When the flow becomes fully developed, the velocity profile in the microchannel is expressed as:

$$V_z(x,y) = \frac{16}{\pi^2\eta}\left(-\frac{dp}{dz} + f_\omega\right)$$

$$\sum_{m=1}^{\infty}\sum_{n=1}^{\infty}\frac{(-1)^{m+n}}{(2m-1)(2n-1)\lambda_{m,n}}\cos\frac{\beta_m x}{a}\cos\frac{\beta_n y}{b}$$

$$(5)$$

The average velocity inside the microchannel could be calculated with the following equation:

$$V_{avg} = \frac{1}{4ab}\int_{-a}^{a}\int_{-b}^{b} V_z(x,y)dxdy = \frac{64}{\pi^4\eta}\left(-\frac{dp}{dz} + f_\omega\right)$$

$$\sum_{m=1}^{\infty}\sum_{n=1}^{\infty}\frac{1}{(2m-1)^2(2n-1)^2\lambda_{m,n}}$$

$$(6)$$

So the flow rate of the steady flow is:

$$Q = 4abV_{\text{avg}}$$

$$= \frac{256ab}{\pi^4\eta}\left(-\frac{\mathrm{d}p}{\mathrm{d}z} + f_\omega\right)\sum_{m=1}^{\infty}\sum_{n=1}^{\infty}\frac{1}{(2m-1)^2(2n-1)^2\lambda_{m,n}} \qquad (7)$$

From Eq. (7), it is noted that the flow rate depends on the dimensions of the microchannel, the pressure gradient, and the centrifugal force in the fluid. In terms of control of the sample volume, this flow rate formula (Eq. (7)) based on the present 3D analysis provides a more accurate prediction than that based on 2D analysis. The smaller the ratio of width to depth of the microchannel, the bigger the discrepancy 2D analysis will cause.

2.2   Pressure Distribution in The Channel

For a steady and continuous centrifugal flow, pressure distribution inside the microchannel is non-uniform. Based on Eq. (2), it is known that the term, $-\mathrm{d}p/\mathrm{d}z + f_\omega$, depends on z only. In addition, the flow rate is independent of z due to flow continuity which indicates $-\mathrm{d}p/\mathrm{d}z + f_\omega$ should be a constant. There must be a resulting pressure gradient, $-\mathrm{d}p/\mathrm{d}z$, to make the term $-\mathrm{d}p/\mathrm{d}z + f_\omega$ constant. Thus,

$$-\mathrm{d}p/\mathrm{d}z + f_\omega = C \qquad (8)$$

where C is a constant which is equivalent to the reduced pressure gradient, G^*, in reference [18].

At $z = r_2 - r_1$, the outlet of the microchannel, the pressure could be assumed to be zero. At $z = 0$, the inlet of the microchannel, the apparent hydrostatic pressure is P_0:

$$P_0 = \int_{r_0}^{r_1} \rho\omega^2 r\,\mathrm{d}r = \frac{1}{2}\rho\omega^2(r_1^2 - r_0^2) \qquad (9)$$

Integrating Eq. (8) from $z = 0$ to $z = r_2 - r_1$, one obtains:

$$C = \frac{1}{2}\rho\omega^2\left(\frac{r_2^2 - r_0^2}{r_2 - r_1}\right) = \rho\omega^2\frac{r_1 + r_2}{2} + \frac{P_0}{r_2 - r_1} \qquad (10)$$

It is noted that C depends on geometric parameters of the flow system, such as r_0, r_1, and r_2. Intuitively, the larger the microchannel length ($r_2 - r_1$), the faster the liquid flows. However, the size of the inlet reservoir ($r_1 - r_0$) also plays an important role in determining C. According to Eq. (10), it is also found that the force term, C, can be divided into two parts: one is due to the centrifugal force and is equivalent to the centrifugal force at the middle of the microchannel; the other is due to the apparent hydrostatic pressure from the inlet reservoir. Eq. (10) gives us a clear idea of how to determine configurations of Lab-on-a-CD flow systems. Given all parameters of the flow system shown in Fig. 1, flow rate can be predicted precisely by combining Eq. (10) with Eq. (7). At any point inside the microchannel, the pressure gradient and pressure can be expressed as:

$$\frac{\mathrm{d}p}{\mathrm{d}z} = \rho\omega^2 z - \frac{1}{2}\rho\omega^2\left(\frac{r_1^2 - r_0^2}{r_2 - r_1} + r_2 - r_1\right) \qquad (11)$$

$$p(z) = \frac{1}{2}\rho\omega^2\left[z^2 - \left(\frac{r_1^2 - r_0^2}{r_2 - r_1} + r_2 - r_1\right)z + (r_1^2 - r_0^2)\right] \qquad (12)$$

Counter-intuitively, the resulting pressure is not linearly distributed, but has a parabolic distribution along the microchannel with a minimum value at $z = \frac{1}{2}\left(\frac{r_1^2 - r_0^2}{r_2 - r_1} + r_2 - r_1\right)$.

2.3   Motion of The Capillary Front in The Microchannel

During a loading process, the most significant feature of the centrifugal microflow is that a moving solid-liquid-vapor interface exists at the front of the liquid plug (Fig. 2), which is also called capillary flow. Capillary flow was first investigated by Lucas [25] and Washburn [26]. Subsequent research studied effects of inertia, [27–29] and energy dissipation [30] on capillary penetration. In addition to these effects, the effect of the dynamic contact angle (Fig. 2) on centrifugal capillary flow is also considered in this model.
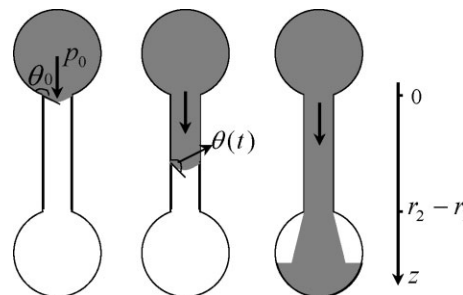

Figure 2. Schematic of the loading process (from left to right): flow is pinned at the entrance of the microchannel by the capillary burst valve; the centrifugal capillary flow advances in the microchannel; and the flow reaches the outlet reservoir and becomes a continuous flow.

As the speed of rotation increases from zero, liquid in the inlet reservoir is supposed to flow into the microchannel due to the centrifugal force. If the inner surface of the microchannel is hydrophobic, the liquid will be pinned at the entrance of the microchannel until the accumulative centrifugal force (Eq. (9)) in the inlet reservoir overcomes the capillary force (Fig. 2). Thus, the capillary force functions as a "valve". In Fig. 2, θ_0 is the static contact angle and $\theta(t)$ is the dynamic contact angle.

By balancing the accumulative centrifugal force (Eq. (9)) and the capillary force at the entrance of the microchannel (Fig. 2), one can obtain the so-called "burst frequency" for this junction [5–16]:

$$\omega = \sqrt{\frac{2c\sigma\cos(180° - \theta_0)}{\rho s(r_1^2 - r_0^2)}} \qquad (13)$$

where c is the length of the contact line between the microchannel and the front of the capillary flow, σ is the liquid-air

Chem. Eng. Technol. **2008**, *31*, No. 9, 1328–1335

Lab-on-a-CD systems   1331

surface tension, and *s* is the cross sectional area of the microchannel. If and only if the rotation frequency exceeds the burst frequency, the liquid can be loaded into the microchannel. Based on the concept of this function, flow valving and sequencing can be realized by modifying surface properties [31, 32], adjusting the rotation speed or changing the channel size.

Once the rotation frequency is larger than the burst frequency, the loading process starts which is time-dependent, and depends on the hydrophobicity of the microchannel surface and the dynamic contact angle at the solid-liquid-vapor interface (Fig. 2). Study of this loading process has a great impact on flow timing and flow sequencing in Lab-on-a-CD systems. There are four competing forces acting on the liquid plug during the entire loading process: (1) the centrifugal force applied to each fluid element; (2) the capillary force at the moving front; (3) the wall shear stress; (4) the apparent hydrostatic pressure or the accumulative centrifugal force (Eq. (9)). The centrifugal force and the apparent hydrostatic pressure cause liquid motion when the CD rotates. The wall shear stress retards the flow. The capillary force always exists at the three-phase (solid-liquid-vapor) contact line in the microchannel during the entire loading process until the capillary front reaches the end of the microchannel (Fig. 2). The capillary force may either enhance flow ($\theta(t) < 90°$) or resist flow ($\theta(t) > 90°$). During the entire loading process, the dynamic contact angle varies with the velocity of the capillary front. The dynamic contact angle should be considered here since the velocity of the liquid plug does vary dramatically at the beginning of the loading process.

During the loading process, the Newtonian dynamics equation can be used to describe flow behavior of the liquid plug:

$$\rho s \frac{\mathrm{d}}{\mathrm{d}t}\left[z(t)\frac{\mathrm{d}z(t)}{\mathrm{d}t}\right] = F_\omega + F_s + F_v + P_0 s \tag{14}$$

where F_ω, F_s and F_v are respectively the centrifugal force, the capillary force, and the wall shear force, which are all imposed on the liquid plug. P_0 is the apparent hydrostatic pressure expressed by Eq. (9). F_ω and F_s are expressed as:

$$F_\omega = 4ab\int_0^z \rho\omega^2(r_1 + z)\mathrm{d}z = 2ab\rho\omega^2 z(2r_1 + z) \tag{15}$$

$$F_s = c\,\sigma\cos,\theta(t) \tag{16}$$

When $\frac{\mathrm{d}z}{\mathrm{d}t}\frac{\eta}{\sigma}$ is larger than 10^{-3}, the relationship between the dynamic contact angle and the static contact angle is given by [33, 34]:

$$\frac{\cos\theta_0 - \cos\theta(t)}{\cos\theta_0 + 1} = 2\left(\frac{\mathrm{d}z}{\mathrm{d}t}\frac{\eta}{\sigma}\right)^{0.5} \tag{17}$$

Otherwise, the following correlation should be used [33]:

$$\frac{\cos\theta_0 - \cos\theta(t)}{\cos\theta_0 + 1} = 4.47\left(\frac{\mathrm{d}z}{\mathrm{d}t}\frac{\eta}{\sigma}\right)^{0.42} \tag{18}$$

The flow in the liquid plug is assumed to be a laminar flow. Thus, the wall shear force can be obtained based on Eq. (3):

$$
\begin{aligned}
F_v &= 2\int_{-b}^{b}\eta\frac{\partial V}{\partial x}\bigg|_{x=a}z\mathrm{d}y + 2\int_{-a}^{a}\eta\frac{\partial V}{\partial y}\bigg|_{y=b}z\mathrm{d}x\\
&= \frac{256zab}{\pi^4}\left(-\frac{\mathrm{d}p}{\mathrm{d}z}+f_\omega\right)\sum_{m=1}^{\infty}\sum_{n=1}^{\infty}\frac{(-1)(1-e^{-\lambda_{m,n}vt})}{(2m-1)^2(2n-1)^2}
\end{aligned}
\tag{19}
$$

Note that the flow rate is:

$$Q_t = 4ab\frac{\mathrm{d}z}{\mathrm{d}t} \tag{20}$$

So the viscous drag force can be expressed as:

$$F_v = -4ab\eta z\frac{\mathrm{d}z}{\mathrm{d}t}\frac{\displaystyle\sum_{m=1}^{\infty}\sum_{n=1}^{\infty}\frac{(1-e^{-\lambda_{m,n}vt})}{(2m-1)^2(2n-1)^2}}{\displaystyle\sum_{m=1}^{\infty}\sum_{n=1}^{\infty}\frac{(1-e^{-\lambda_{m,n}vt})}{(2m-1)^2(2n-1)^2\lambda_{m,n}}} \tag{21}$$

Given an angular velocity, for a moving capillary front which has traveled a distance *z*, the Newton dynamics equation is:

$$
\begin{aligned}
4ab\rho\left[z\frac{\mathrm{d}^2z}{\mathrm{d}t^2}+\left(\frac{\mathrm{d}z}{\mathrm{d}t}\right)^2\right] &= 2ab\rho\omega^2 z(2r_1+z) + c\sigma\cos\theta(t)\\
&+ 2ab\rho\omega^2(r_1^2-r_0^2)\\
&- 4ab\eta z\frac{\mathrm{d}z}{\mathrm{d}t}\frac{\displaystyle\sum_{m=1}^{\infty}\sum_{n=1}^{\infty}\frac{(1-e^{-\lambda_{m,n}vt})}{(2m-1)^2(2n-1)^2}}{\displaystyle\sum_{m=1}^{\infty}\sum_{n=1}^{\infty}\frac{(1-e^{-\lambda_{m,n}vt})}{(2m-1)^2(2n-1)^2\lambda_{m,n}}}
\end{aligned}
\tag{22}
$$

or

$$
\begin{aligned}
\frac{\mathrm{d}^2z}{\mathrm{d}t^2} &= \omega^2\left(r_1+\frac{z}{2}\right) + \frac{c\sigma\cos\theta(t)}{4\rho abz} + \frac{1}{2z}\omega^2(r_1^2-r_0^2) - \frac{\eta}{\rho}\frac{\mathrm{d}z}{\mathrm{d}t}\\
&\frac{\displaystyle\sum_{m=1}^{\infty}\sum_{n=1}^{\infty}\frac{(1-e^{-\lambda_{m,n}vt})}{(2m-1)^2(2n-1)^2}}{\displaystyle\sum_{m=1}^{\infty}\sum_{n=1}^{\infty}\frac{(1-e^{-\lambda_{m,n}vt})}{(2m-1)^2(2n-1)^2\lambda_{m,n}}} - \frac{1}{z}\left(\frac{\mathrm{d}z}{\mathrm{d}t}\right)^2
\end{aligned}
\tag{23}
$$

The corresponding initial conditions are: $z(0) = z_0$, $\mathrm{d}z(0)/\mathrm{d}t = 0$ and $\theta(0) = \theta_0$. To avoid singularity, z_0 is set a very small distance instead of zero. In numerical simulation, $\theta(t)$ is determined by either Eq. (17) or Eq. (18) according to the velocity of the capillary front.

3   Parametric Study and Discussion

The model described in the preceding section is expected to be a useful design tool for Lab-on-a-CD systems. In this section, to illustrate the features and applicability of the model, it is utilized to generate the flow behavior data for some typical design of Lab-on-a-CD systems. In all of these calculations, the

working fluid is assumed to be water but not limited to water, and these parameters are used in parametric analysis: $\rho = 10^3$ kg/m^3, $\sigma = 72.5 \cdot 10^{-3}$ N/m, $\eta = 0.89 \cdot 10^{-3}$ Pa·s. The variables are microchannel geometry, the contact angle, and locations of the reservoirs.

3.1 Pressure Distribution along The Microchannel

After the capillary front travels through the microchannel and reaches the outlet reservoir (Fig. 2), the flow becomes continuous and finally, a steady flow. The resulting pressure distribution along the microchannel depends on geometric parameters of the flow system such as size and location of the inlet reservoir, and size and length of the microchannel. According to Eq. (12), there are two categories of pressure distribution. If $r_0^2 \leq 2 r_1 r_2 - r_2^2$, the resulting pressure decreases monotonically along the streamwise of the microchannel; while if $r_0^2 > 2 r_1 r_2 - r_2^2$, the resulting pressure decreases first and then increases. At the critical point, $z = \frac{1}{2}(\frac{r_1^2 - r_0^2}{r_2 - r_1} + r_2 - r_1)$, the pressure reaches its minimum value (Fig. 3).

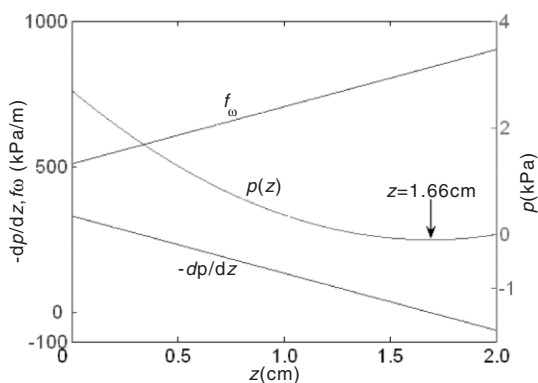**Figure 3.** Pressure distribution along the microchannel, where $\omega = 140$ rad/s, $r_0 = 2$ cm, $r_1 = 2.6$ cm, and $r_2 = 4.6$ cm. At $z = 1.66$ cm, the pressure reaches its minimum.

3.2 Time-Dependent Behavior of Fluid Flow in The Microchannel

In this section, the following parameters are used unless specified: $2a = 80$ μm, $2b = 50$ μm, $r_0 = 2$ cm, $r_1 = 2.6$ cm, $r_2 = 3.6$ cm, and the static contact angle, $\theta_0 = 120°$, which is referred to the contact angle of deionized water on a UV or ethanol-treated poly(dimethylsiloxane) (PDMS) surface [35–37]. The initial condition is set as $z_0 = 10$ nm.

Manipulation of time dependence of flow is important to many microfluidic functions, such as flow timing and flow sequencing. In this section, time-dependent behaviors of capillary flows in microchannels are investigated. Based on Eq. (13) and the parameters introduced above, the burst frequency of the flow system is 130.7 rad/s, so that angular velocities used in the following parametric studies are larger than 130.7 rad/s.

Fig. 4 shows the effect of the angular velocity on the capillary flow where the travel length of the advancing capillary flow is set as 1 cm. As expected, the time-dependent motion of the capillary flow is strongly affected by the angular velocity. As the angular velocity increases from 140 rad/s to 160 rad/s, the advancing velocity increases from 0.093 m/s to 0.129 m/s, the peak speed of the flow "burst" increases from 0.268 m/s to 0.826 m/s, and the loading time reduces from 0.112 s to 0.068 s. For all the angular velocities used here, the liquid plug extends along the microchannel at a nearly constant speed after the transient "burst" which indicates that the driving forces are nearly balanced by resisting forces. In fact, the total centrifugal force is only slightly larger than the summation of the capillary force and the wall shear force. It is a useful feature that the advancing speed remains almost constant within most part of the travel span which provides researchers a simple method to estimate flow timing in designing Lab-on-a-CD devices (i.e., the microchannel length divided by the constant advancing speed is approximately the loading time).
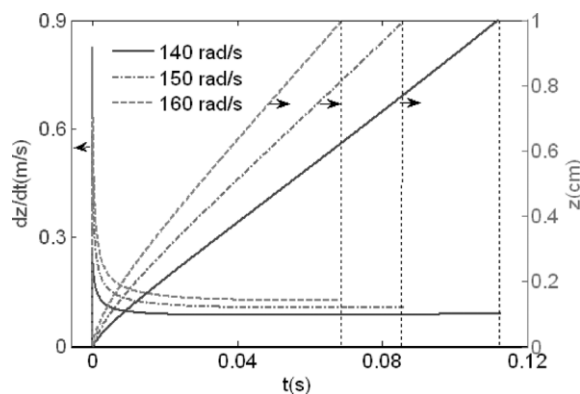

Figure 4. Time-dependent behavior of the moving front at different angular velocities, where $r_0 = 2$ cm, $r_1 = 2.6$ cm, and $r_2 = 3.6$ cm (the travel span of the fluid is confined to a 1 cm-long microchannel).

When the disk rotates at an angular velocity of 140 rad/s, the capillary front can reach the outlet reservoir in 0.112 s and the final speed of the capillary front (0.093 m/s) is smaller than the average speed of the corresponding continuous flow at steady state, where $V_{avg} = 0.126$ m/s is obtained by using Eq. (6). This indicates that the capillary flow has not fully developed before the fluid reaches the outlet reservoir at the end of the microchannel. If the length of the microchannel is extended up to 2 cm, the capillary front will reach the outlet reservoir in 0.218 s, and the final speed of the capillary front will become 0.103 m/s (Fig. 5) which is closer to the average velocity of the corresponding continuous flow ($V_{avg} = 0.121$ m/s). If the microchannel length is further extended, the capillary flow will become fully developed before reaching the outlet reservoir. As for the velocity, a longer microchannel does not necessarily lead to a larger velocity which also depends on size and location of the inlet reservoir.
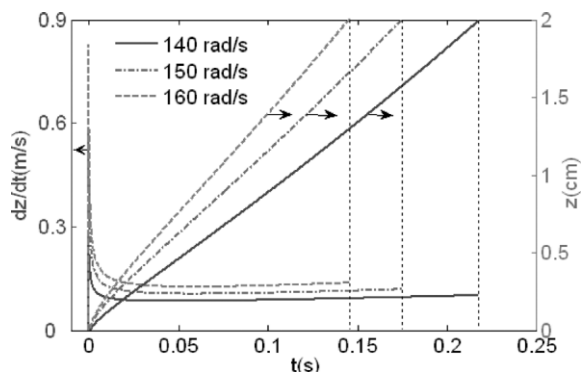
Figure 5. Time-dependent behavior of the moving front at different angular velocities, where $r_0 = 2$ cm, $r_1 = 2.6$ cm, and $r_2 = 4.6$ cm (the travel span of the fluid is confined to a 2 cm-long microchannel).

Figure 7. Effect of the size of the microchannel on time-dependent behavior of the moving front, where $\omega = 170$ rad/s, $r_0 = 2$ cm, $r_1 = 2.6$ cm, and $r_2 = 3.6$ cm.

The advancing speed of the capillary front also depends on the size and location of the inlet reservoir which provides an apparent hydrostatic pressure to the liquid plug (see Fig. 2). As shown in Fig. 6, the farther the microchannel locates from the center of rotation, the larger the centrifugal force the liquid plug receives. Thus, both the total driving force and the advancing speed of the capillary front are raised. Fig. 7 shows the effect of the microchannel size on flow velocity. The advancing speed of the capillary front increases as the dimension of the microchannel increases (see Fig. 7). This is because the effect of the capillary force on the flow becomes weaker as the microchannel dimension increases.
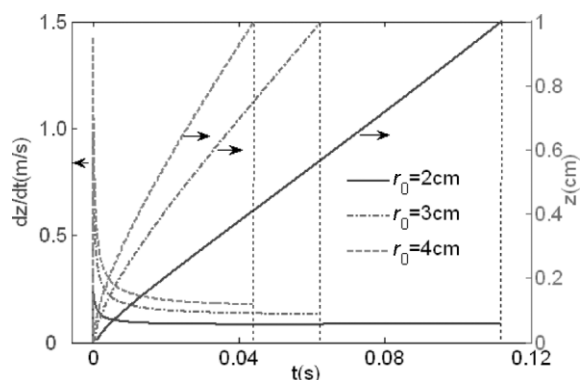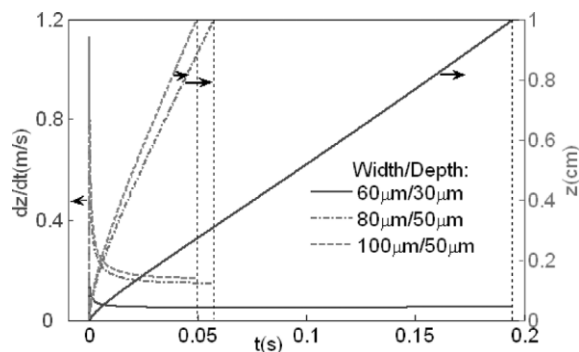

Figure 8. Effect of hydrophobicity (or static contact angles θ_0) of the microchannel on time-dependent behavior of the moving front, where $\omega = 140$ rad/s, $r_0 = 2$ cm, $r_1 = 2.6$ cm, and $r_2 = 3.6$ cm.
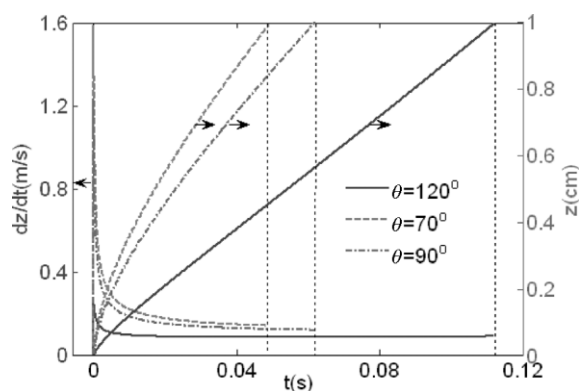

Figure 6. Effect of the position of the inlet reservoir on time-dependent behavior of the moving front, where $\omega = 140$ rad/s, $r_1 = r_0 + 0.6$ cm, and $r_2 = r_0 + 1.6$ cm.

In addition, the advancing velocity is also affected by hydrophobicity of the inner surface of the microchannel. As shown in Fig. 8, a more hydrophobic surface causes more resistance to the flow. When the surface is hydrophilic (e.g., $\theta_0 = 70°$), the model is still valid. But there will be no "capillary valve" at the microchannel entrance, thus no "flow burst" phenomenon. The dynamic characteristics of the contact angle play an important role, since the contact angle actually becomes larger

with the increase of flow velocity. For example, when $\omega = 140$ rad/s, the final velocity with consideration of the dynamic contact angle will be 0.014 m/s smaller than that without consideration of the dynamic contact angle effect. However, if the angular velocity is much larger than the burst frequency, the effect of the capillary force will become smaller since the centrifugal force will dominate the loading process.

All of the results above show that the advancing speed of the capillary front has a sharp increase at the beginning of the loading process, and then decreases quickly. This special flow phenomenon has indeed been observed experimentally and is commonly referred to as "flow burst". To the best of the authors' knowledge, this is the first time that "flow burst" is modeled theoretically. Accordingly, it is interesting to further explore the "flow burst" characteristics. In reality, when a "flow burst" is formed, only a very small volume of liquid penetrates into the microchannel at the beginning of the loading process and the acceleration of the liquid penetration is actually very large at this time. One can imagine that a finite force is applied on an infinitely small liquid element. This phenomenon can be reflected theoretically using Eq. (23). Given a small initial

length of liquid ($z(t = 0_+) = z_0$) and $\dfrac{dz(0_+)}{dt} = 0$, the initial acceleration speed can be obtained from Eq. (23):

$$\left.\frac{d^2z}{dt^2}\right|_{t=0_+} = \omega^2\left(r_1 + \frac{z_0}{2}\right) + \frac{c\sigma\cos\theta_0}{4\rho abz_0} + \frac{1}{2z_0}\omega^2(r_1^2 - r_0^2) \qquad (24)$$

Assuming that z_0 is very small, one can find that the second and third terms on the right side of Eq. (24) are huge numbers. Thus, the initial acceleration could be very large which causes apparently a "flow burst".

3.3 Concept of Digital Flow Control

More importantly, the phenomena of the flow burst and centrifugal capillary flows predicted by this model have a significant impact on digital microfluidics, which instead of continuous microflows, is accepted as the next generation Lab-on-a-chip technology [5–12]. In order to realize this function, one can increase the angular velocity above the burst frequency and stop the rotation suddenly at a given time, such that the liquid plug inside the microchannel is of a well-controlled volume, and can be separated from the liquid in the inlet reservoir. The model proposed here can provide guidance to the design of digital Lab-on-a-CD devices. For example, the size of the microchannel and locations of reservoirs, angular velocities to be applied, volume of the liquid plug inside the microchannel, and the time to stop rotation can be predicted by this model.

In addition, the flow burst shows a special advantage in generating ultrafine droplets. In principle, a certain kinetic energy is required for a liquid plug to separate from the liquid in the inlet reservoir. The longer the liquid plug, the more kinetic energy it has, but the bigger its volume. Due to the high ejecting speed of the flow burst, a short liquid plug may have enough kinetic energy to make a break.

4   Conclusions

A theoretical model for determining time-dependent flow behaviors in a 3D rotating rectangular microchannel is proposed for Lab-on-a-CD devices. The velocity profile, flow rate, the moving capillary front, and the pressure distribution along the microchannel are characterized. Effects of the geometric parameters of Lab-on-a-CD systems on flow behaviors are investigated. It is found that the advancing speed of the capillary front depends on the angular velocity, locations of reservoirs, and dimension, location, and surface properties of the microchannel. The mechanism of "flow burst" at the beginning of the loading process is first physically described and determined. More importantly, this model provides many insights into digital microfluidic control in Lab-on-a-CD systems. In conclusion, this model is of practical significance in prediction of centrifugal microflows and the design of Lab-on-a-CD systems for various applications of analytical chemistry.

Symbols used

V_x, V_y, V_z	[m s^{-1}]	flow velocity in x, y, z direction
V_{avg}	[m s^{-1}]	average flow velocity inside the microchannel
x, y, z	[m]	coordinates of the microchannel system
t	[s]	time
p	[Pa]	pressure in the microchannel
a, b	[m]	half of width and depth of the microchannel
r	[m]	distance from the center of the CD
f_ω	[N m^{-3}]	centrifugal force density
f_c	[N m^{-3}]	Coriolis force density
Q_t	[m^3 s^{-1}]	flow rate at time t
Q	[m^3 s^{-1}]	flow rate of steady flow
C	[N m^{-3}]	a constant
$-dp/dz$	[Pa m^{-1}]	pressure gradient along the microchannel
F_ω	[N]	centrifugal force
F_s	[N]	capillary force
F_v	[N]	wall shear force
dz/dt	[m s^{-1}]	advancing speed of the capillary front

Greek symbols

v	[m^2 s^{-1}]	liquid kinetic viscosity
η	[Pa s]	liquid viscosity
σ	[N m^{-1}]	liquid-air surface tension
ω	[s^{-1}]	angular velocity of the CD
θ	[–]	contact angle at the liquid-solid-gas interface
ρ	[kg m^{-3}]	density of the fluid

References

[1] D. J. Harrison et al., *Science* **1993**, *261*, 895.

[2] D. J. Harrison, A. Van den Berg, *Micro Total Analysis Systems '98*, Kluwer Academic Publishers, Boston **1998**.

[3] A. Manz, H. Becker, *Microsystem Technology in Chemistry and Life Sciences*, Springer-Verlag, Berlin **1998**.

[4] O. Geschke, H. Klank, P. Tellemann, *Microsystem Engineering of Lab-on-a-Chip Devices*, WILEY-VCH, Weinheim **2004**.

[5] M. J. Madou et al., *Biomed. Microdevices* **2001**, *3*, 245.

[6] D. C. Duffy et al., *Anal. Chem.* **1999**, *71*, 4669.

[7] R. Zengerle, P. Koltay, J. Ducrée, *15th Int. Sym. on Micro-Nanomechatronics and Human Science*, Nagoya, Japan, **2004**.

[8] M. Grumann et al., *Rev. Sci. Instrum.* **2005**, *76 (2)*, 025101.

Chem. Eng. Technol. **2008**, *31*, No. 9, 1328–1335

Lab-on-a-CD systems   1335

[9] G. J. Wang, W. H. Hsu, Y. Z. Chang, H. Yang, *Biomed. Micro-devices* **2004**, *6*, 47.

[10] J. Kim et al., *Lab Chip* **2004**, *4*, 516.

[11] S. Lai et al., *Anal. Chem.* **2004**, *76*, 1832.

[12] T. Berner, T. Glatzel, R. Zengerle, J. Ducrée, *Lab Chip* **2005**, *5*, 146.

[13] H. S. Cho, H. Y. Kim, J. Y. Kang, T. S. Kim, *J. Colloid Interface Sci.* **2007**, *306*, 379.

[14] Y. K. Cho et al., *Lab Chip* **2007**, *5*, 565.

[15] J. M. Park et al., *Lab Chip* **2007**, *5*, 557.

[16] S. K. Lee, G. R. Yi, S. M. Yang, *Lab Chip* **2006**, *9*, 1171.

[17] G. S. Benton, D. Boyer, *J. Fluid Mech.* **1966**, *26*, 69.

[18] G. Marliani, M. Matzkeit, V. I. Vasanta Ram, *Exp. Fluids* **1997**, *23*, 64.

[19] S. N. Baura, *Proc. R. Soc. London Ser. A.* **1954**, *227*, 133.

[20] G. S. Benton, *Trans. ASME, J. Appl. Mech.* **1956**, *23*, 123.

[21] K. S. Yang, J. Kim, *Phys. Fluids A.* **1991**, *3*, 633.

[22] U. Lei, C. H. Hsu, *Phys. Fluids A.* **1990**, *2*, 63.

[23] J. V. Beck, *Heat Conduction Using Green's Functions*, Hemisphere, London, **1992**.

[24] J. Yang, D. Y. Kwok, *J. Chem. Phys.* **2003**, *118*, 354.

[25] R. Lucas, *Colloid. Polym. Sci.* **1918**, *23*, 15.

[26] E. W. Washburn, *Phys. Rev.* **1921**, *17*, 273.

[27] C. H. Bosanquet, *Philos. Mag.* **1923**, *45*, 525.

[28] A. A. Duarte, D. E. Strier, D.H. Zanette, *Am. J. Phys.* **1996**, *64*, 413.

[29] D. Quéré, *Europhys. Lett.* **1997**, *39*, 533.

[30] G. L. Batten, *J. Colloid Interface Sci.* **1984**, *102*, 513.

[31] S. Prakash et al., *Anal. Chem.* **2007**, *79*, 1661.

[32] B. J. Kirby, E. F. Hasselbrink, *Electrophoresis* **2004**, *25*, 187.

[33] J. E. Seebergh, J. C. Berg, *Chem. Eng. Sci.* **1992**, *47*, 4455.

[34] J. C. Berg, *Wettability*, Marcel Dekker, New York **1993**.

[35] K. G. Marinova et al., *Langmuir* **2005**, *21*, 11729.

[36] J. M. Uilk, A. E. Mera, R. B. Fox, K. J. Wynn, *Macromolecules* **2003**, *36*, 3689.

[37] A. Mata, A. J. Fleischman, S. Roy, *Biomed. Microdevices* **2005**, *74*, 281.